LA-UR-13-26664
Approved for public release; distribution is unlimited.

Title: Hydropolis Dam Failure: Impact Assessments

Author(s): Bent, Russell W.
Brelsford, Christina M.
Tasseff, Byron A.
Visarraga, Darrin B.

Intended for: 12th International Benchmark Workshop on Numerical Analysis of Dams, 2013-10-02/2013-10-04 (Graz, Austria)

Issued: 2013-08-23

Hydropolis Dam Failure: Impact Assessments

Russell Bent, Christa Brelsford, Byron Tasseff, and Darrin Visarraga

Los Alamos National Laboratory, Energy and Infrastructure Analysis Group, Los Alamos, New Mexico, USA

E-mail: btasseff@lanl.gov

ABSTRACT

One of the major challenges facing urban planners is the problem of how to assess risk associated with potential natural disasters. The challenge increases in difficulty when the scenarios considered by planners lack historical precedent. This is often the case for scenarios associated with dam failures, as these are atypical occurrences. While the scientific community has made tremendous strides in developing simulation models of dam failures, their accuracy remains dependent on the accuracy of the input parameters to the model. More importantly, perhaps, the results of dam failure simulations (flood characteristics) are used for consequence assessment such as population at risk, loss of life, and direct economic impacts.

To address this concern, this paper surveys the possible input parameters to such models and tests the parameters on the Hydropolis dam failure scenario. The dam failure results are then used to calculate consequence. Interestingly, while the range of possible inputs is considerable, the range in consequence is much smaller. This suggests that consequence assessment for dam failure is surprisingly robust to error in the input parameters. Finally, this methodology allows planners to understand the range of possible outcomes and plan accordingly.

INTRODUCTION

Over the past 100 years or more, modern civilization has increasingly relied on a vast complex of dams to control the behavior of rivers and streams. These dams are used to generate power, reduce the risk of seasonal flooding, support agriculture, and provide clean drinking water. However, these dams introduce risk in the form of failure and subsequent downstream flooding. Thankfully, these events are rare, so planners and engineers rely on computational models and simulations to predict the outcome and consequence of dam failures. As the availability of multi-processor computing techniques has significantly increased over the past decade, these models have become increasingly sophisticated and realistic. However, the ability to benchmark and validate such tools, in particular for risk assessment, remains a difficult challenge.

This challenge motivates Theme C of the 12th International Benchmark Workshop on Numerical Analysis for Dams. The numerical problem proposed for Theme C focuses on estimating the consequences of a dam failure near a populated area with complex demographics, infrastructure, and economic activity. This paper addresses Theme C by making the following contributions:

- A survey of input parameters used in two-dimensional (2D) flood modeling
- An ensemble of possible outcomes based on the survey
- A consensus based approach for choosing input parameters in the absence of validation data

- A methodology for estimating population at risk (PAR), loss of life (LOL), and direct gross domestic product (GDP) impacts within the downstream inundated areas

FLOOD INUNDATION

Methodology and Literature Review

Historically, flood inundation has been simulated using one-dimensional (1D) flow models with predefined channels [1]. Although such methods are numerically simple, data development for 1D model inputs can be costly and time-consuming [2]. Additionally, 1D models cannot simulate more complex flows because lateral diffusion is neglected [3]. Recent advances in computational resources have made more sophisticated models, like 2D models, tractable. Although 2D models are more complex to develop and implement, they allow for higher precision results and the simulation of more nuanced floodplains, including urban areas. Moreover, 2D models may utilize (with little to no preprocessing) a wide range of increasingly available, high-resolution topographic data [4].

Based on these observations, we used the 2D inundation model[1] described by Kurganov and Petrova to simulate the Hydropolis dam breach [5]. Their approach numerically approximates the 2D shallow water equations using a central-upwind, finite-volume method to spatially discretize and solve the system under consideration. For the temporal discretization, we used a second-order total variation diminishing Runge-Kutta scheme. The code also employed wet cell tracking, allowing processors to avoid unnecessary computations in dry regions. We validated the code using a variety of scenarios described throughout the literature, including those described in [6], [7], [8], [9], and [10]. In each validation example, results were found to be of similar or of higher quality than what had been documented in the literature.

A key challenge in flood modeling is parameterizing the simulation. In particular, models are sensitive to dam breach and roughness parameters. To account for such sensitivity, we produced 15 simulations of the Hydropolis dam break to estimate variances introduced by different selections of breach parameters and land type/roughness values. For these simulations, we implemented supercritical flow conditions along the four domain boundaries and used the supplied digital elevation model (DEM) including the dam. We modeled the dam breach as a point source located slightly downstream of the dam, near the location (4687.89 m, 6778.68 m). For each simulation, we used unit flow data to produce the five required cross-sectional hydrographs. For each hydrograph, unit flow was integrated over each linear cross-section, those endpoints are defined in Table 1. We then used similarity metrics among the results to determine the submitted result.

Table 1. Points defining the five required hydrograph cross-sections

Cross Section ID	Point 1		Point 2	
	x (m)	y (m)	x (m)	y (m)
1	4,800.05	6,911.55	4,800.05	6,541.41
2	5,913.56	7,297.84	6,026.31	6,835.74
3	7,436.01	7,833.57	7,514.87	7,491.00
4	9,131.61	8,102.21	9,065.07	7,375.17
5	10876.32	7779.35	10553.47	7015.35

[1] Implemented on a GPU using NVIDIA's CUDA architecture

Breach Parameter Assumptions

We used the five breach parameter estimation methods provided in the scenario documentation and the supplied dam property descriptions to obtain the set of breach parameters listed in Table 2.

Table 2. Comparison of breach parameters used to describe the Hydropolis dam failure

Breach Parameter	[11]	[12]	[13]	[14] (erosion resistant)	[14] (easily erodible)
B_w (m)	4.91	61.79	49.47	146.4	146.4
t_f(s)	6601.62	2362.07	2046.88	5292.0	3294.0

In addition to breach parameter estimations, there are a variety of methods for generating breach discharge hydrographs. In this study, we applied the widely used National Weather Service DAMBRK model [15]. This model approximates breach outflow as broad-crested weir flow; in units of cubic meters per second, it is described by Equation 1:

$$Q_{breach} = c_v k_s \left(3.1 b_i (h - h_b)^{3/2} + 2.45 Z (h - h_b)^{5/2}\right) \quad (1)$$

where c_v is a velocity of approach correction, b_i is the instantaneous breach bottom width, h is the water surface elevation upstream of the dam, h_b is the elevation of the breach bottom, Z is the side slope of the breach, and k_s is a submergence correction due to downstream tailwater elevation. Because the scenario did not provide information concerning downstream tailwater, we assumed k_s to be unity. The velocity of approach correction is computed in Equation 2:

$$c_v = 0.5521 + 0.041661 \frac{Q_i^2}{B_d^2 (h - h_{bm})^2 (h - h_b)} \quad (2)$$

where B_d is the reservoir width at the dam and h_{bm} is the terminal breach bottom elevation. The results of the five breach parameters are described in Figure 1. It is important to note that the peak discharges, both in terms of discharge rate and timing of the peak, vary by a factor of 3. This illustrates the need for accurate parameterization of the breach discharge.

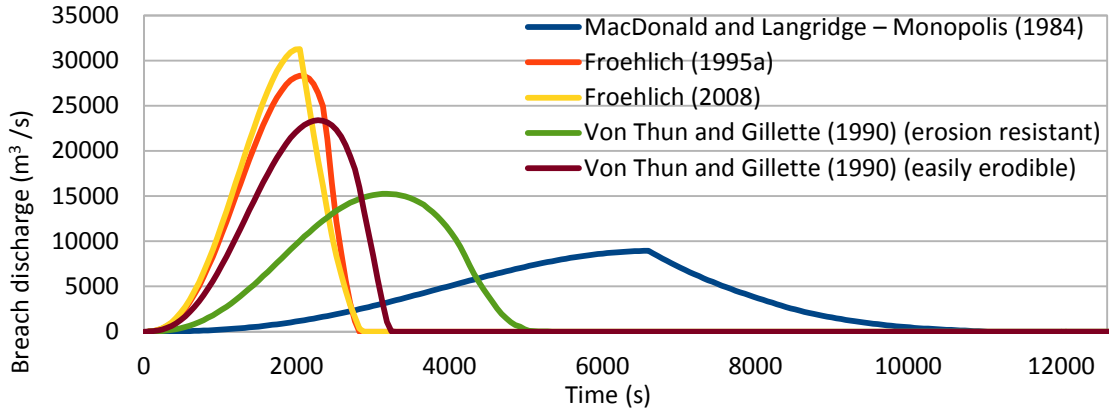

Figure 1. Comparison of estimated breach discharge hydrographs using the five breach parameterization methodologies provided in ICOLD's Theme C documentation

Land Roughness Assumptions

Roughness is an important parameter influencing surface flow patterns in inundation models [16], [17], but it is also one of the most variable and uncertain. While land use/land cover (LULC) data may allow for the automatic parameterization of a domain's roughness,

variability may present itself through a multitude of systematic errors. Land types may be misclassified or classified differently across multiple references, local land types may differ substantially when compared to nationally categorized land types, and roughness may be measured (or calibrated) differently across references.

Without historical data of previous Hydropolis inundation events, an empirically based calibration procedure to estimate LULC correlations with local roughness values could not be developed. Instead, we conducted a literature review of land type/roughness correlations, which revealed a wide range of possible parameters (Table 3).

Table 3. Comparison of Manning roughness coefficients for 2001 NLCD land types, defined by a selection of literature; with trimmed mean roughness coefficients (i.e., the mean of values excluding extrema)

NLCD Class	Description	[16]	[18]	[19]	[20]	[21]	[22]	[23]	Trimmed Mean
11	Open Water	0.037	0.020	0.03	0.020	0.0010	0.030	0.06	0.027
21	Developed - Open	0.048	0.020	0.013		0.0404	0.035	0.010	0.027
22	Developed - Low		0.050	0.05	0.120	0.0678	0.015	0.010	0.046
23	Developed - Med.		0.100	0.075		0.0678	0.015	0.010	0.053
24	Developed - High	0.022	0.150	0.1	0.121	0.0404	0.015	0.010	0.060
31	Barren Land	0.026	0.090	0.03	0.040	0.0113	0.035	0.035	0.033
41	Deciduous Forest		0.100	0.12	0.160	0.36	0.1	0.070	0.120
42	Evergreen Forest	0.050	0.110	0.12	0.180	0.32	0.1	0.070	0.116
43	Mixed Forest		0.100	0.12	0.170	0.40	0.1		0.123
52	Shrub/Scrub	0.043	0.050	0.05	0.070	0.40	0.035	0.055	0.054
71	Grassland/Herbaceous	0.022	0.034	0.03	0.035	0.368	0.035	0.050	0.037
81	Pasture/Hay	0.045	0.033	0.04	0.033	0.325	0.035	0.040	0.039
82	Cultivated Cropland		0.037	0.035	0.040		0.035	0.040	0.037
90	Woody Wetlands	0.037	0.100	0.1	0.140	0.086	0.070		0.089

Given the range of possible Manning coefficients, we conducted numerous simulations to determine the sensitivity of the output to error when selecting these values. Here, we computed the second maximum, second minimum, and trimmed mean roughness values for each 2001 NLCD classification. In principle, minimal and maximal parameters provide boundaries on possible outcomes, while trimmed mean parameters produce roughly “average” results. Second minima and maxima were used due to abnormally large and small extreme points. These three sets of values were combined with the breach parameters (15 total simulations). Future work will consider a broader set of parameter choices and develop statistical methods for combining results.

Analysis of Results

To provide a sensitivity analysis of simulation results, we ran several simulations based on a variety of parameters. The lack of historical data resulted in a limited set of options for the analysis of simulation results. We could not use historic events in similar regions as baselines for roughness or dam breach parameter calibration because the dam location is not provided in the scenario. As a result, the most defensible approach was to consider the set of possible outcomes based on the possible parameter settings in order to understand the range and

variability of the results, but the rules of this workshop require us to submit a single result. In the absence of calibration data, an "average" or median result, taken as a function of roughness and dam breach conditions collected over a variety of locations, is generally an acceptable approach, so we considered a number of analytical techniques to assess consensus. For ease of comparison, we assigned numerical labels to each unique set of parameters used in the simulations and described in Table 4.

Table 4. Labels and descriptions of parameters used in the Hydropolis simulations

Run Label	Breach Parameterization	Roughness
1	Von Thun and Gillette (1990), Erosion Resistant	Trimmed Mean
2	Von Thun and Gillette (1990), Easily Erodible	
3	Froehlich (2008)	
4	Froehlich (1995)	
5	MacDonald and Langridge-Monopolis (1984)	
6	Von Thun and Gillette (1990), Erosion Resistant	Second Minimum
7	Von Thun and Gillette (1990), Easily Erodible	
8	Froehlich (2008)	
9	Froehlich (1995)	
10	MacDonald and Langridge-Monopolis (1984)	
11	Von Thun and Gillette (1990), Erosion Resistant	Second Maximum
12	Von Thun and Gillette (1990), Easily Erodible	
13	Froehlich (2008)	
14	Froehlich (1995)	
15	MacDonald and Langridge-Monopolis (1984)	

The first comparison method was the "fit" of flooded areas among simulation results, a statistic presented by Bates and De Roo [24] (Equation 3):

$$F^{(2)} = \frac{A_{obs} \cup A_{mod}}{A_{obs} \cap A_{mod}} \tag{3}$$

where A_{obs} and A_{mod} are the total inundation areas of observed and modeled data, respectively. A fit value of unity implies a perfect fit, while a fit value of zero implies no fit. As all simulation results were modeled, this statistic was computed 15^2 times, labeling each result as "observed" and "modeled" 15 times. These analyses resulted in a matrix of $F^{(2)}$ values, depicted in Figure 2a.

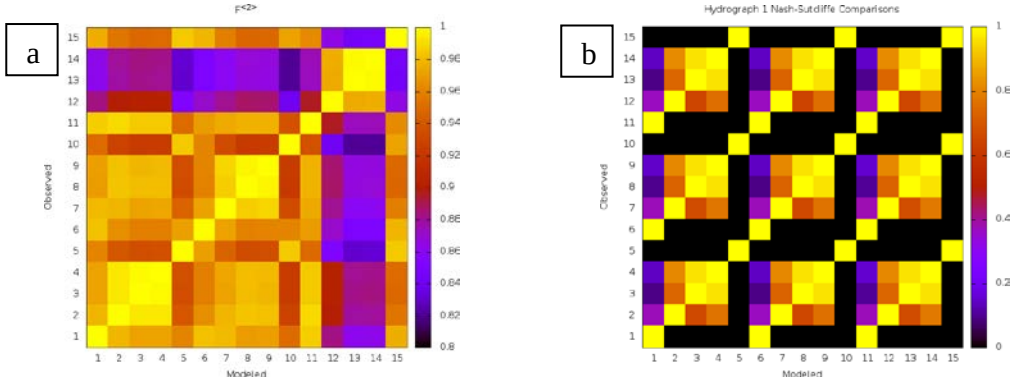

Figure 2. (a) Matrix of Bates and De Roo fit statistics; (b) Matrix of Nash-Sutcliffe efficiency coefficients, comparing simulated cross-sectional hydrographs "1"

The second comparison method was the computation of Nash-Sutcliffe model efficiency coefficients [25], calculated upon comparing cross-sectional discharge hydrographs to one another. The Nash-Sutcliffe coefficient is defined by Equation 4:

$$E = 1 - \frac{\sum_{t=0}^{T}(Q_{obs}^{t} - Q_{mod}^{t})^2}{\sum_{t=0}^{T}\left(Q_{obs}^{t} - \overline{Q_{obs}}\right)^2} \quad (4)$$

where Q_{obs}^{t} and Q_{mod}^{t} are observed and modeled discharges at time *t*, and $\overline{Q_{obs}}$ is the mean observed discharge. An efficiency of 1 indicates a perfect fit of modeled to observed data, while efficiencies less than zero imply the observed mean provides a better predictor than the model. We computed this statistic 15^2 times for each of the five compared cross-sectional hydrographs, labeling each result as "observed" or "modeled." Matrices similar to that of Figure 2a were generated to compare the Nash-Sutcliffe coefficients; the matrix comparing cross-sectional hydrographs "1" is shown pictorially in Figure 2b. Matrices describing the four other cross-sectional hydrographs were similar.

For the third comparison method, we constructed a mean peak flood depth grid and subsequent comparisons with simulated peak flood depth grids. The mean peak flood depth grid was produced after averaging peak flood depths for each simulated cell. Simulated peak flood depth grids were then compared to the mean peak flood depth grid, and the root-mean-square error (RMSE) was computed as in Equation 5:

$$RMSE = \sqrt{\frac{\sum_i \sum_j \left(\overline{h_{ij}^{peak}} - h_{ij}^{peak}\right)^2}{N\left(\overline{A} \cup A\right)}} \quad (5)$$

where $\overline{h_{ij}^{peak}}$ and h_{ij}^{peak} are the averaged and simulated peak heights at grid cell C_{ij}, respectively, and $N\left(\overline{A} \cup A\right)$ is the number of cells contained by the union of the averaged and simulated flooded areas. Similar comparisons were also performed using peak unit discharge grids. The results of these analyses are summarized in Table 5.

Table 5. Computed RMSE values, comparing averaged peak flood depth, and averaged peak unit discharge grids to simulated grids

Run Label	Peak Flood Depth RMSE (m)	Peak Unit Discharge RMSE (m^2/s)
1	0.344097	3.463832
2	0.238518	1.568955
3	0.541395	5.542898
4	0.446684	4.088387
5	0.798121	7.353910
6	0.603485	3.452673
7	0.322903	2.760809
8	0.366026	6.742362
9	0.314924	5.237147
10	1.003072	7.303872
11	0.226322	3.789764
12	0.539361	1.660771
13	0.846326	5.028675
14	0.763336	3.723210
15	0.614361	7.463132

Comparing the fit statistics displayed in Figure 2a showed that trimmed mean and minimum roughness simulation results compared favorably, while maximum roughness results were markedly different. We summed the fit statistics for each run, and found that Run 2 provided the largest amount of "fit" among the set of results.

Figure 2b displays the results of comparing cross-sectional hydrographs at cross-section ID 1. We observed similar patterns for cross-sectional hydrographs 2 through 5, although coefficient values varied with distance from the breach source (a consequence of varying roughness). This comparison implied that discharges measured at the specified locations were more strongly related to breach discharge hydrographs than roughness coefficients. To classify parameters that provided consistently similar results, we summed the number of occurrences where the Nash-Sutcliffe coefficient was greater than zero. Using this measure, the Von Thun and Gillette (easily erodible) parameters provided the most similar results, with Von Thun and Gillette (erosion resistant) parameters closely trailing. Simulation Run 6 provided the most consistent results overall.

Table 5 describes simulated data deviations compared to mean data grids. Naturally, the mean grids produced were biased toward roughness parameters and breach hydrographs that were similar to one another. The values displayed in Table 5 implied that RMSE was reduced near trimmed mean roughness values, but also that Von Thun and Gillette (easily erodible) breach parameters provided the best agreement to mean grids across all three sets of roughness parameters. Run 11 produced the smallest peak depth RMSE, while Run 2 produced the smallest peak unit flow RMSE.

Taking all methods of comparison into account, the best parameter choice used trimmed mean roughness values and Von Thun and Gillette (easily erodible) breach parameters (i.e., Run 2). We chose results from this simulation for submission.

CONSEQUENCE ASSESSMENT

A full-scale dam failure risk assessment generally includes the following four categories: public health and safety, economic impact, psychological impact, and governance/mission impact. In this study, the analyses focused on PAR, LOL, and direct GDP impacts.

Population at Risk

PAR is the total projected number of people occupying a permanent residence, a commercial building, or a recreational area within a potential flooded zone. Capturing reasonable approximations of the population that could be severely affected by the flood is the primary goal in estimating potential human impacts linked to a specific flood event.

Methodology: One challenge in computing PAR is resolving spatial resolution differences between population data (e.g., census data) and simulated flood data. Additionally, disaggregating spatial population data across census tracts is another challenge often encountered in calculating PAR. One approach to resolving these challenges is to disaggregate the spatial data uniformly across all census tracts. In densely populated settings where census tracts cover small areas, such an approach tends to work well. However, this approach is less reliable in sparsely populated regions, where people cluster in communities and along road networks and where census tracts cover large areas, leaving most of the area in any tract essentially unpopulated. As Hydropolis contains many unpopulated areas, a more precise method is needed to obtain a better representation of where the population is located. There are two approaches to using remote sensing data to obtain a more accurate spatial

representation of population within census tracts. One involves the use of night-time lights [26], and the other uses impervious surfaces [27], which cannot be penetrated by water. Examples include compacted clay, roads, parking lots, sidewalks, and driveways. As these examples suggest, impervious surfaces are often associated with urban and suburban areas. We used the latter approach to yield a reasonable proxy for densely populated areas.

In this study, we used the supplied LULC data for impervious surfaces, and the population of Hydropolis was uniformly distributed over all impervious surfaces located within each census tract. Data on parcels, which included information on area zoning (e.g., residential, commercial, industrial) and building structures (e.g., number of stories, basement, and quality), was also provided for this study, but we did not use it for the population distribution adjustment. This population redistribution approach can overlook people located within tracts that do not contain any impervious surfaces. In the supplied census dataset, 116 tracts did not contain any impervious surfaces; these tracts contained about 6% of the study area population. A vast majority of these tracts are at an elevation higher than the dam breach, so although these residents are not included in the spatial analyses, the missing population is not expected to have any effect on the consequence analysis results.

To estimate the PAR in different levels of flooding, we overlaid a spatial grid of total population with a peak flood depth grid (based on the impervious surface disaggregation approach). We used the same procedure to estimate the PAR based on different flood wave arrival times—the population grid is overlaid with a grid of wave arrival times, and the population at risk is binned into categories based on flood arrival times.

Analysis of Results: Over the 15 model runs, the inundation area ranged from 64 km^2 to 78 km^2, yielding a PAR range of approximately 21,000 to 28,000. Using Run 2 as the base scenario, results yielded a total flooded area of 69.3 km^2 and a PAR of 26,520. Figure 3 shows the spatial variability of PAR for Run 2, regardless of age, for Hydropolis. Figure 4 shows the variability of PAR based for all simulations.

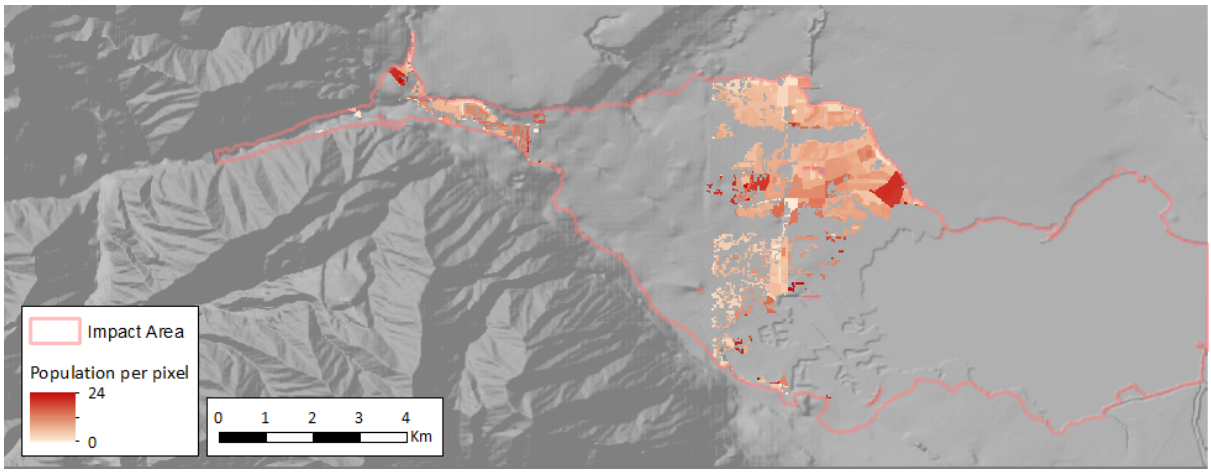

Figure 3. Spatial variability of total PAR for Run 2

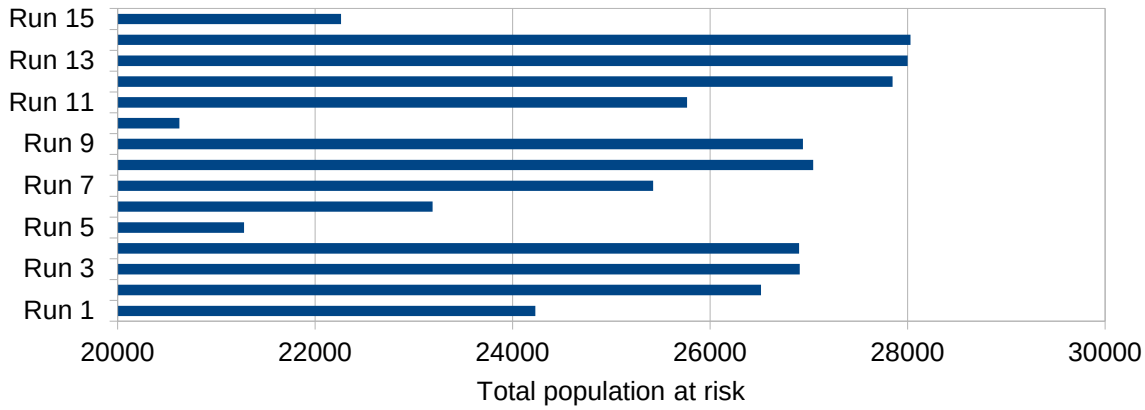

Figure 4. Comparison of total PAR for all simulation runs

Loss of Life

Methodology: The second consequence metric considered in this study is loss of life. This approach is based on the methodology developed by E. Penning-Rowsell, et al., in [28], which considers three factors: (1) flood hazard, (2) area vulnerability, and (3) people vulnerability. Flood hazard ratings are derived from depth, velocity, and debris characteristics of the flood. The area vulnerability factor is based on the effectiveness of a flood warning system for an area, the speed of onset of the flood, and the land use characteristics or zoning of the area (e.g., residential homes, multi-story apartments, commercial/industrial properties, mobile homes). The people vulnerability factor is based on the degree to which people are exposed to the flood, and the number of infirm/disabled and senior people in the at risk population [29].

To estimate loss of life for the different flood wave arrival times, we generated spatial grids for hazard ratings, area vulnerability (i.e., flood warning, speed of onset, nature of area) and people vulnerability (i.e., elderly (65 years and older) and infirm/disabled/sick). Assuming a uniform debris field factor of 1 (i.e., possible), we calculated hazard rating grids using estimated flood depths and velocity spatial grids. Based on the estimated flood arrival times, we determined the flood warning and speed of onset grids using the values listed in Table 6.

Table 6. Flood warning and speed of onset raster values

Zone Area	Time Interval (seconds)	Cell Value
Flood Warning Raster		
High Risk	0 < Time <= 3600	3
Med Risk	3600 < Time <= 7200	2
Low Risk	Time > 7200	1
Speed of Onset Raster		
High Risk	0 < Time <= 1800	3
Med Risk	1800 < Time <= 5400	2
Low Risk	Time > 5400	1

Using the supplied benchmark parcel data, we computed the nature of the area spatial grid using a similar process. We assumed that the number of stories assigned to each structure was uniform, and we used this attribute and the values listed in [28] to determine each grid cell value.

Analogous to the area vulnerability grids, the people vulnerability grids were determined based on the supplied benchmark census data. Census tract percentage values for the elderly were compared against corresponding percentage values for Hydropolis and assumed to be around the national average. This corresponded to a medium risk parameter selection for the people vulnerability grids. We used the parameter values listed in [28] to determine the grid cell values for the elderly and infirm/disabled/sick spatial grids.

Analysis of Results: Given an estimated inundation area in the range of 64 square km to 78 square km, the estimated total loss of life impacts range from 345 to 2084. Note that these range estimates were taken over all 15 simulations. Table 7 lists the total loss of life estimates within the indicated flood wave arrival time intervals for Run 2.

Table 7. Loss of life estimates, per flood arrival times, for Run 2

Flood Arrival Time (min)	Loss of Life
0–15	0
15–30	145
30–60	626
60–90	232
90–120	26
120–180	5
> 180	2
Total	1036

Direct Gross Domestic Product Impact

Methodology**:** The number of affected jobs by job category is estimated using a methodology analogous to that used for PAR. We assume a job is affected if the employee is no longer earning a wage and job activity is assumed to stop if the job is located in a grid cell that has any level of flooding. Jobs of all categories were uniformly distributed over impervious surfaces within each census tract, and the affected jobs were then calculated based on the intersection between the jobs grid and the flood arrival time grid.

We generated direct GDP per employee per day for each job category based on the 2010 United States National Average GDP, the North American Industry Classification System (NAICS) codes, the U.S. Bureau of Economic Analysis, and the U.S. Bureau of Labor Statistics data. These numbers were used to estimate direct GDP impact from affected jobs. Table 8 shows these values. We estimated the direct GDP impact of the flood on Hydropolis by multiplying the number of affected jobs in each category by the GDP/employee/day for each category. We then computed a summation of these product values over all job categories.

Infrastructure damages caused by flooding are considered insured or uninsured asset loss, hence, dollar estimates associated with infrastructure damages are not included in these direct GDP impact estimates. Additionally, infrastructure value data was not provided as part of the benchmark specifications, and any estimate of the value of insured or uninsured losses would be governed by assumptions made about the value of the infrastructure.

Table 8. Direct GDP per employee day values by job category

NAICS Code	NAICS	Field Name	GDP/Employee/Day ($)
21	Mining	jobs21	553.52
22	Utilities	jobs22	1,253.28
23	Construction	jobs23	157.25
31-33	Manufacturing	jobs3133	381.98
42	Wholesale Trade	jobs42	361.35
44-45	Retail Trade	jobs4445	136.48
48-49	Transportation and Warehousing	jobs4849	200.35
51	Information	jobs51	532.02
52	Finance and Insurance	jobs52	352.55
53	Real Estate and Rental and Leasing	jobs53	648.36
54	Professional, Scientific, and Technical Services	jobs54	255.98
55	Management of Companies and Enterprises	jobs55	354.50
56	Administrative and Support and Waste Management and Remediation Services	jobs56	110.69
61	Educational Services	jobs61	109.61
62	Health Care and Social Assistance	jobs62	159.42
71	Arts, Entertainment, and Recreation	jobs71	100.91
72	Accommodation and Food Services	jobs72	94.76
81	Other Services (except Public Administration)	jobs81	99.15
92	Government	jobs92	206.32

Analysis of Results: Over the 15 model runs, the 24 hour direct GDP impact varied between $340,000 and $620,000. Table 9 presents direct GDP impact estimates within the indicated flood wave arrival time intervals and shows the range of results for direct economic activity at risk.

Table 9. Direct GDP impact estimates, per flood arrival time.

Flood Arrival Time (min)	Direct GDP Impact ($USD/day)
0–15	0
15–30	86,618
30–60	108,257
60–90	263,295
90–120	79,256
120–180	18,930
> 180	120
Total	556,476

CONCLUSION

One of the biggest engineering achievements of the past century or more is the ability of modern society to control the flow of rivers through the use of dams. These dams reduce the risk of seasonal flooding, produce electric power, and provide agricultural benefits. However these dams introduce risk to downstream population and assets that requires evaluation. This paper surveys recent advances in dam failure modeling and the associated input parameters. These input parameters were evaluated on the Hydropolis dam failure scenario and used to

calculate consequence. Interestingly, while the range of possible inputs was considerable, the range in consequence was much smaller. This suggests that consequence assessment for dam failure is surprisingly robust to error in the input parameters. However, despite these results there are a number of opportunities for future work. In particular, it will be important to improve techniques used to determine appropriate input parameters in the absence of calibration data. To address this challenge, we have conducted an additional 150 model runs and plan to use their impact results to build a statistical approximation to the simulator like the one described in [30] for a problem domain with similar characteristics. This approximation, called an emulator, allows thorough exploration of the model inputs and outputs. This will allow us to conduct detailed sensitivity studies and bound the set of inputs that give physically reasonable responses. The emulator will also be used to calibrate input settings when physical data are available; and we will demonstrate this capability in the context of the Hydropolis problem when the "real" outcome is revealed.

ACKNOWLEDGEMENTS

The authors would like to acknowledge Earl Lawrence for his guidance on statistical methods, Lisa Inkret for her valuable comments, and James Arnold for his GIS expertise.

REFERENCES

[1] D. L. Fread, "Channel routing," in *Hydrological Forecasting*, John Wiley and Sons Ltd., 1985, pp. 437–503.

[2] K. Bradbrook, "JFLOW: a multiscale two-dimensional dynamic flood model," *Water and Environment Journal*, vol. 20, no. 2, pp. 79–86, 2006.

[3] A. J. Kalyanapu, S. Shankar, E. R. Pardyjak, D. R. Judi and S. J. Burian, "Assessment of GPU computational enhancement to a 2D flood model," *Environmental Modelling & Software*, vol. 26, no. 8, pp. 1009–1016, 2011.

[4] D. R. Judi, "Fast response flood estimation model documentation report," Technical Report, 2008.

[5] A. Kurganov and G. Petrova, "A second-order well-balanced positivity preserving central-upwind scheme for the Saint-Venant system," *Communications in Mathematical Sciences*, vol. 5, no. 1, pp. 133–160, 2007.

[6] F. Alcrudo and P. Garcia-Navarro, "A high-resolution Godunov-type scheme in finite volumes for the 2D shallow-water equations," *International Journal for Numerical Methods in Fluids*, vol. 16, no. 6, pp. 489–505, 1993.

[7] A. R. Brodtkorb, M. L. Sætra and M. Altinakar, "Efficient shallow water simulations on GPUs: Implementation, visualization, verification, and validation," *Computers & Fluids*, vol. vol. 55, pp. 1–12, 2012.

[8] R. Holdahl, H. Holden and K. A. Lie, "Unconditionally stable splitting methods for the shallow water equations," *BIT Numerical Mathematics*, vol. 39, no. 3, pp. 451–472, 1999.

[9] L. Cea, M. Garrido and J. Puertas, "Experimental validation of two-dimensional depth-averaged models for forecasting rainfall-runoff from precipitation data in urban areas," *Journal of Hydrology*, vol. 382, no. 1, pp. 88–102, 2010.

[10] A. Chertock, S. Cui, A. Kurganov and T. Wu, “Well-balanced positivity preserving central-upwind scheme for the shallow water system with friction terms,” *Journal of Computational Physics*, submitted.

[11] T. C. MacDonald and J. Langridge-Monopolis, “Breaching charateristics of dam failures,” *Journal of Hydraulic Engineering*, vol. 110, no. 5, pp. 567–586, 1984.

[12] D. C. Froehlich, “Peak outflow from breached embankment dam,” *Journal of Water Resources Planning and Management*, vol. 121, no. 1, pp. 90–97, 1995.

[13] D. C. Froehlich, “Embankment dam breach parameters and their uncertainties,” *Journal of Hydraulic Engineering*, vol. 134, no. 12, pp. 1708–1721, 2008.

[14] J. L. Von Thun and D. R. Gillette, “Guidance on breach parameters,” Unpublished manuscript, U.S. Bureau of Reclamation, Denver, Colorado1990.

[15] D. L. Fread, “The NWS DAMBRK model: Theoretical background/user documentation,” Hydrologic Research Laboratory, National Weather Service, NOAA, 1988.

[16] S. C. Medeiros, S. C. Hagen and J. F. Weishampel, “Comparison of floodplain surface roughness parameters derived from land cover data and field measurements,” *Journal of Hydrology*, 2012.

[17] M. Straatsma, “3D float tracking: in situ floodplain roughness estimation,” *Hydrological Processes*, vol. 23, no. 2, pp. 201–212, 2009.

[18] C. Mattocks and C. Forbes, “A real-time, event-triggered storm surge forecasting system for the state of North Carolina,” *Ocean Modelling*, vol. 25, no. 3, pp. 95–119, 2008.

[19] M. R. Moore, Development of a high-resolution 1D/2D coupled flood simulation of Charles City, Iowa, 2011.

[20] S. Bunya, J. Dietrich, J. Westerink, B. Ebersole, J. Smith, J. Atkinson, R. Jensen, D. Resio, R. Luettich, C. Dawson and et. al., “A high-resolution coupled riverine flow, tide, wind, wind wave, and storm surge model for southern Louisiana and Mississippi. Part I: Model development and validation,” *Monthly Weather Review*,vol. 138, no. 2, pp. 345–377, 2010.

[21] A. J. Kalyanapu, S. J. Burian and T. N. McPherson, “Effect of land use-based surface roughness on hydrologic model output,” *Journal of Spatial Hydrology*, vol. 9, no. 2, 2010.

[22] B. E. Vieux, B. E. Vieux, Distributed hydrologic modeling using GIS, Springer, 2001.

[23] M. Hernandez, S. N. Miller, D. C. Goodrich, B. F. Goff, W. G. Kepner, C. M. Edmonds and K. B. Jones, “Modeling runoff response to land cover and rainfall spatial variability in semi-arid watersheds,” in *Monitoring Ecological Condition in the Western United States*, Springer, 2000, pp. 285–298.

[24] P. Bates and A. De Roo, “A simple raster-based model for flood inundation simulation,” *Journal of hydrology*, vol. 236, no. 1, pp. 54–77, 2000.

[25] J. E. Nash and J. V. Sutcliffe, “River flow forecasting through conceptual models part I: A discussion of principles,” *Journal of Hydrology*, vol. 10, no. 3, pp. 282–290, 1970.

[26] C. D. Elvidge, K. E. Baugh, S. J. Anderson, P. C. Sutton and T. Ghosh, “Elvidge, C. D., Baugh, K. E., Anderson, S. J., Sutton, Paul C., and Ghosh, T.:(2012) The Night Light Development Index (NLDI): a spatially explicit measure of human development from satellite data,” *Social Geography*, vol. 7, pp. 23–35, 2012.

[27] D. Lu, Q. Weng and G. Li, “Residential population estimation using a remote sensing derived impervious surface approach,” *International Journal of Remote Sensing*, vol. 27, no. 16, pp. 3553–3570, 2006.

[28] E. Penning-Rowsell, P. Floyd, D. Ramsbottom and S. Surendran, “Estimating Injury and Loss of Life in Floods: A Deterministic Framework,” *Natural Hazards*, vol. 36, no. 1–2, pp. 43–64. 2005.

[29] S. Larsen, D. Judi, S. Del Valle, J. Ambrosiano and T. N. McPherson, “Modeling the Impact of a Patient Surge,” ESRI, 2011.

[30] E. Lawrence, K. Heitmann, M. White, D. Higdon, C. Wagner, S. Habib and B. Williams, “The Coyote Universe III: Simulation Suite and Precision Emulator for the Nonlinear Matter Power Spectrum,” *The Astrophysical Journal*, vol. 713, pp. 1322–1331, 2010.

[31] N. Crawford and R. Linsley, “Digital simulation in hydrology: Stanford watershed model 4,” Technical Report/Department of Civil Engineering. Stanford University, 1966.

[32] J. Singh, M. S. Altinakar and Y. Ding, “Two-dimensional numerical modeling of dam-break flows over natural terrain using a central explicit scheme,” *Advances in Water Resources*, vol. 34, no. 10, pp. 1366–1375, 2011.

[33] R. H. McCuen, Hydrologic analysis and design, Englewood Cliffs, NJ: Prentice-Hall, 1989.